Ingenieur-Archiv 59 (1989) 160–174

Ingenieur-Archiv

Numerical methods for bifurcation analysis in geomechanics*

R. de Borst, Delft

Summary: A numerical approach to bifurcation problems in soil plasticity is outlined. While previously published results have been obtained using non-associated plasticity models, results are now presented for strain-softening plasticity. Attention is focused on a biaxial test, for which results have been obtained starting from a perfectly homogeneous sample and for a sample that contains imperfections. It is shown that the mere introduction of an imperfection not always transfers a bifurcation problem into a limit problem. This observation illustrates the need for an option in a finite element program that carries out a bifurcation analysis.

Numerische Methoden zur Verzweigungsanalyse in der Bodenmechanik

Übersicht: Skizziert wird eine numerische Behandlung von Verzweigungsproblemen in der Plastizität von Böden. Während frühere Ergebnisse für nicht-assoziiertes plastisches Verhalten gewonnen wurden, werden hier solche für entfestigendes Verhalten dargestellt. Das Hauptaugenmerk ist auf einen zweiachsigen Versuch gerichtet. Für ihn werden Ergebnisse beschrieben in den Fällen, daß von einer vollständig homogenen Probe bzw. einer Probe mit Imperfektionen ausgegangen wird. Es wird gezeigt, daß die alleinige Einführung von Imperfektionen nicht immer ein Verzweigungsproblem in ein Grenzlastproblem überführt. Diese Beobachtung zeigt die Notwendigkeit, daß Finite-Element-Programme eine Option zur Durchführung von Verzweigungsanalysen enthalten sollten.

1 Introduction

Failure in soil masses is often accompanied by a sudden transition of a smoothly varying deformation field into a number of highly localized deformation bands. These so-called shear bands occur virtually at the peak of the load-displacement diagram and a drop in this diagram is usually observed once the shear bands start propagating.

Some ten years ago it was recognized that this problem must be formulated as a bifurcation problem [1–4]. Within this framework it proved possible to analytically derive formulae for the critical hardening modulus at which bifurcation into a localized deformation band is first possible and for the angle between the deformation band and the principal stress axes. Computation of the post-bifurcation behavior, however, is not possible using analytical tools, and it is here that a numerical approach offers new possibilities. In metal plasticity this approach was pioneered by Needleman and Tvergaard (e.g. [5, 6]), who analyzed a wide variety of problems involving necking and shear banding. The extension to soil plasticity was made by Prévost [7, 8] and de Borst and Vermeer [9–11], while applications to crack problems in concrete have also been published recently [12–14].

Within the context of soil plasticity, it seems natural to first consider the biaxial test, since much analytical work has been devoted to this type of experiment. A profound understanding of the phenomena that are observed in this experiment has been gained, which allows a careful examination of the numerical results. This was done in a previous publication for a material

* Presented at the workshop on Limit Analysis and Bifurcation Theory, held at the University of Karlsruhe (FRG), February 22–25, 1988

model that assumed strain-hardening, non-associated Mohr-Coulomb plasticity. This analysis yielded a good qualitative agreement with test results, but a number of questions remained. The inability to give a rigorous answer to these questions partly relates to the non-symmetric character of the tangential stiffness matrix that is generated by a non-associated plasticity model. In the present paper attention is therefore devoted to a somewhat simpler material model. By using a strain-softening von Mises plasticity model the problems signalled in [11] can be unraveled somewhat further.

A further point that is addressed in this contribution is whether the ability to recognize and pass bifurcation points in discrete mechanical models is indeed necessary or whether it suffices to simply put some weak spots (imperfections) in the model. It will be shown that relying on imperfections to remove to bifurcation point, i.e. transferring the bifurcation problem into a limit problem, may be dangerous.

2 Uniqueness of discretized mechanical systems

Incremental equilibrium of a structure requires that a stress rate distribution, say $\dot{\boldsymbol{\sigma}}_A$, satisfies

$$\int_V \delta\boldsymbol{\epsilon}^T \dot{\boldsymbol{\sigma}}_A \, \mathrm{d}V = \delta\mathbf{a}^T \dot{\mathbf{F}} \tag{1}$$

for all kinematically admissible virtual strain vectors $\delta\boldsymbol{\epsilon}$. Here $\dot{\mathbf{F}}$ is the rate at which the external forces vary and $\delta\mathbf{a}$ is the virtual displacement vector. At a bifurcation point there must exist yet another stress rate distribution, say $\dot{\boldsymbol{\sigma}}_B$, that satisfies incremental equilibrium. Consequently, $\dot{\boldsymbol{\sigma}}_B$ must also satisfy (1) and subtraction of both equilibrium equations results in

$$\int_V \delta\boldsymbol{\epsilon}^T \, \Delta\dot{\boldsymbol{\sigma}} \, \mathrm{d}V = 0 \tag{2}$$

with $\Delta\dot{\boldsymbol{\sigma}}$ as difference between both stress rate distributions.

We next define $\mathbf{B}$ as the strain-nodal displacement matrix that relates the strain rate vector $\dot{\boldsymbol{\epsilon}}$ to the nodal velocities $\dot{\mathbf{a}}$, i.e.

$$\dot{\boldsymbol{\epsilon}} = \mathbf{B}\dot{\mathbf{a}} \tag{3}$$

and suppose that both stress rate distributions are related to strain rates $\dot{\boldsymbol{\epsilon}}$ by the same tangential relation $\mathbf{D}$:

$$\dot{\boldsymbol{\sigma}} = \mathbf{D}\dot{\boldsymbol{\epsilon}}. \tag{4}$$

Using (3) and (4), (2) can be rewritten as

$$\delta\mathbf{a}^T \int_V \mathbf{B}^T\mathbf{D}\mathbf{B} \, \mathrm{d}V \, \Delta\dot{\mathbf{a}} = 0 \tag{5}$$

or, defining the tangential stiffnes matrix $\mathbf{K}$

$$\mathbf{K} = \int_V \mathbf{B}^T\mathbf{D}\mathbf{B} \, \mathrm{d}V \tag{6}$$

we get

$$\delta\mathbf{a}^T\mathbf{K} \, \Delta\dot{\mathbf{a}} = 0 \tag{7}$$

where $\Delta\dot{\mathbf{a}}$ is the difference between both velocity distributions. Since (7) must hold for any virtual displacement, the following set of equations is to be valid at bifurcation point:

$$\mathbf{K} \, \Delta\dot{\mathbf{a}} = \mathbf{0}. \tag{8}$$

We next write $\Delta\dot{\mathbf{a}}$ as a linear combination of the n right eigenvectors $\mathbf{v}_i$ and the n left eigenvectors $\mathbf{w}_i$ of the matrix $\mathbf{K}$:

$$\Delta\dot{\mathbf{a}} = \sum_{i=1}^{n} (\mathbf{w}_i^T \, \Delta\dot{\mathbf{a}}) \, \mathbf{v}_i. \tag{9}$$

Then (8) can be recast in the form

$$\sum_{i=1}^{n} (\mathbf{w}_i^T \, \Delta\dot{\mathbf{a}}) \, \lambda_i \mathbf{v}_i = \mathbf{0} \tag{10}$$

since $\mathbf{K}\mathbf{v}_i = \lambda_i \mathbf{v}_i$ (no summation implied). Assuming that $\mathbf{K}$ is not defect, the right eigenvectors $\mathbf{v}_i$ and the left eigenvectors $\mathbf{w}_i$ each constitute a set of n linearly independent eigenvectors. Consequently, $(\mathbf{w}_i^T \, \Delta\dot{\mathbf{a}}) \, \lambda_i$ must vanish for each i. Since $\Delta\dot{\mathbf{a}}$ can not be orthogonal to each left eigenvector $\mathbf{w}_i$, this means that at least one eigenvalue, say λ_1, must vanish at a bifurcation point.

In practical numerical analyses a point where the tangential stiffness has exactly one or more vanishing eigenvalues will never be encountered. Instead it is assumed that a bifurcation point has been passed when at least one (slightly) negative eigenvalue is extracted on a monotonically rising part of the load-deflection curve or when two or more negative eigenvalues have been calculated on a descending branch of this curve.

It is emphasized that this derivation has been carried out under the assumption that both stress rates are related to strain rate by the same tangential stress-strain matrix $\mathbf{D}$. Strictly speaking, we have to investigate all combinations of loading and unloading, since, in particular for elastic-plastic solids with a non-associated flow rule, it is not sufficient to investigate only the case that all plastic points remain on the loading branch because of the loss of the variational structure of the field equations.

3 Techniques for analyzing post-failure and post-bifurcation behavior

When a bifurcation point has been detected according to the procedure outlined in the preceding section, the incremental solution $\Delta\mathbf{a}$ can be perturbed by adding a part of the right eigenvector $\mathbf{v}_1$, which corresponds to the lowest eigenvalue λ_1. Note that the Δ symbol now stands for an increment and no longer for the difference between two quantities. In consideration of (9) we obtain for the perturbed displacement increment

$$\Delta\mathbf{a}^* = \Delta\mathbf{a} + \beta(\mathbf{w}_1^T \, \Delta\mathbf{a}) \, \mathbf{v}_1 \tag{11}$$

with β a kind of damping/amplification factor. A value of 0.01 for this factor appeared to yield satisfactory results in numerical experiments.

The tangent stiffness matrix not only possesses zero eigenvalues at bifurcation points, but also at limit points. Both types of behavior may be encountered in a numerical analysis. For instance, in the case of the biaxial test to be discussed in the next sections the limit and bifurcation points are clustered very closely. The most elegant procedure for overcoming limit points is indirect displacement control, which method will be summarized hereafter.

In a non-linear finite element analysis, the load is applied in a number of small increments. Within each load increment, equilibrium iterations are applied and in iteration number i the iterative improvement $\delta\mathbf{a}_i$ to the displacement increment $\Delta\mathbf{a}_{i-1}$ is given by

$$\delta\mathbf{a}_i = \mathbf{K}_{i-1}^{-1} \left(\Delta\lambda_i \mathbf{q}^* + \lambda_0 \mathbf{q}^* - \int_V \mathbf{B}^T \boldsymbol{\sigma}_{i-1} \, \mathrm{d}V \right) \tag{12}$$

where $\mathbf{K}_{i-1}$ is the possibly updated stiffness matrix, $\mathbf{q}^*$ is the normalized load vector, $\Delta\lambda_i$ is the value of the load increment which may change from iteration to iteration and λ_0 is the value of the load parameter at the beginning of the current increment.

The essence of indirect displacement control is that $\delta\mathbf{a}_i$ is thought to be composed of two contributions

$$\delta\mathbf{a}_i = \delta\mathbf{a}_i^{\mathrm{I}} + \Delta\lambda_i \, \delta\mathbf{a}_i^{\mathrm{II}} \tag{13}$$

with

$$\delta\mathbf{a}_i^{\mathrm{I}} = \mathbf{K}_{i-1}^{-1} \left(\lambda_0 \mathbf{q}^* - \int_V \mathbf{B}^T \boldsymbol{\sigma}_{i-1} \, \mathrm{d}V \right), \tag{14}$$

$$\delta\mathbf{a}_i^{\mathrm{II}} = \mathbf{K}_{i-1}^{-1} \mathbf{q}^* . \tag{15}$$

After calculating $\delta \mathbf{a}_i^{\mathrm{I}}$ and $\delta \mathbf{a}_i^{\mathrm{II}}$, $\Delta\lambda_i$ is determined from a constraint equation on the displacement increments and $\Delta \mathbf{a}_i$ is subsequently calculated from

$$\Delta \mathbf{a}_i = \Delta \mathbf{a}_{i-1} + \delta \mathbf{a}_i^{\mathrm{I}} + \Delta\lambda_i \, \delta \mathbf{a}_i^{\mathrm{II}}. \tag{16}$$

In this paper a linearized constraint equation has been adopted (see [10—12, 17]) which results in the following expression for $\Delta\lambda_i$:

$$\Delta\lambda_i = -\frac{\Delta \mathbf{a}_{i-1}^T \, \delta \mathbf{a}_i^{\mathrm{I}}}{\Delta \mathbf{a}_{i-1}^T \, \delta \mathbf{a}_i^{\mathrm{II}}}. \tag{17}$$

For problems that involve localization of deformation the method fails, since then only a few nodes contribute to the norm of displacement increments. Consequently, failure is not sensed accurately by a global norm. The constraint equation is therefore amended by letting it operate only on a subspace of the n-dimensional displacement space. Then (17) changes into

$$\Delta\lambda_i = -\frac{\Delta \mathbf{u}_{i-1}^T \, \delta \mathbf{u}_i^{\mathrm{I}}}{\Delta \mathbf{u}_{i-1}^T \, \delta \mathbf{u}_i^{\mathrm{II}}} \tag{18}$$

where $\Delta \mathbf{u}_i$ contains only a limited number of the degrees-of-freedom of those of $\Delta \mathbf{a}_i$.

In the example of a biaxial test to be discussed in the subsequent sections, the load has been applied to the top of the sample while the magnitude of the load increment was determined by constraining the vertical displacement increment of the top of the sample. Hence, $\mathbf{u}$ contains the vertical displacement of one node at the top of the sample as degree-of-freedom, i.e. $\mathbf{u} = [0, \ldots, u_{\mathrm{top}}, \ldots, 0]^T$, and $\Delta\lambda_i$ is simply computed from

$$\Delta\lambda_i = -\delta u_{\mathrm{top}}^{\mathrm{I}} / \delta u_{\mathrm{top}}^{\mathrm{II}}.$$

Constraint equations, also named dependence relations in the sequel, in which the other vertical displacements of the top of the sample are forced to follow δu_{top}, the vertical displacement of the master degree-of-freedom, have been added to the system of equations so as to ensure that all the vertical displacements of the nodes at the top were equal.

4 Connections with previous work

Let us proceed by reviewing some results that have been the subject of the previous publications [10, 11]. In these publications, a biaxial test was also analyzed, but a cohesionless sand was considered. The material model adopted was a Mohr-Coulomb plasticity model with a non-associated flow rule. Such a model results in a non-symmetric tangential stress-strain relation, which is numerically inconvenient when decomposing the tangent stiffness matrix and even more when calculating eigenvalues.

The calculations started from a strain-free sample with an isotropic initial stress state. Subsequently, the axial load was increased until a (slightly) negative eigenvalue was extracted for the tangent stiffness matrix, or in other words, when the tangent stiffness matrix ceased to be positive definite. The solution was then perturbed according to the procedure described in the preceding section.

The eigenmode that corresponds to the lowest eigenvalue at the bifurcation point has been plotted in Fig. 1. This eigenmode raises some questions. First, the eigenmode bears similarity with a diffuse bifurcation mode with an arbitrarily short wavelength, but it certainly does not resemble a localized shear band mode, which should theoretically also be available at this point [18, 19]. Secondly, the wavepattern that is displayed by this mode neither shows symmetry nor does it show antisymmetry. A possible explanation suggested in [11] is that the round-off error, which is difficult to avoid when calculating eigenvectors for non-symmetric matrices with many degrees-of-freedom, prevents the computation of an accurate eigenvector. Another explanation suggested in [11] is that there exist more (slightly) negative eigenvalues at this point, because several bifurcation points are clustered very closely along the equilibrium path. In fact, Needleman [20] has pointed out that symmetric and antisymmetric modes with an arbitrarily short

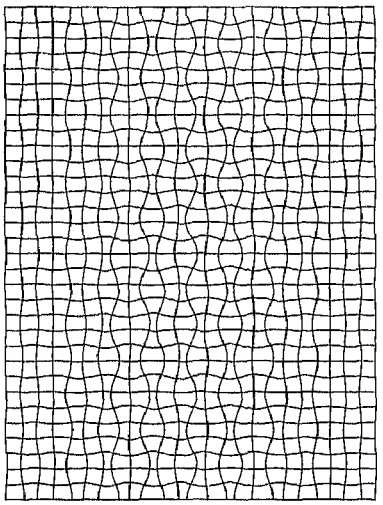

Fig. 1. Eigenmode that belongs to the lowest eigenvalue at bifurcation for biaxial test on dry sand (Mohr-Coulomb plasticity with a non-associated flow rule)

wavelength are both available within the hyperbolic regime. Since, for small deformation gradients as considered here, such modes first become available at the elliptic-hyperbolic boundary, symmetric and antisymmetric eigenmodes are available at this point. Combinations of symmetric and antisymmetric modes are then also eigenvectors, and an eigenvalue analysis of the stiffness matrix at such a point results in an eigenvector which is an arbitrary linear combination of symmetric and antisymmetric modes. A definite answer could not be provided to this question, since the lowest eigenvalue of this non-symmetric matrix has been extracted using a power method. This procedure can only extract the lowest eigenvalue and corresponding eigenvector. For symmetric matrices, more accurate methods exist which, in addition, can simultaneously extract several eigenvalues [21].

5 Material model used in present analyses

In the analyses to be described in the following sections, a simple von Mises strain-softening plasticity model with an associated flow rule has been used. The yield function is given by

$$f = \sqrt{3J_2} - \sigma_y(\varkappa) \tag{19}$$

with J_2 the second invariant of the deviatoric stress tensor and σ_y the current yield stress which is a function of the strain hardening parameter $\varkappa$. In view of the fact that the von Mises yield function has been used, the choice of the expression for $\varkappa$ becomes irrelevant. While in the analysis that was recalled in the preceding section, loss of ellipticity of the governing field equations was caused by the use of a non-associated flow rule, this is now achieved by making σ_y a descending function of the hardening parameter $\varkappa$ (Fig. 2). The problems that are generated by using a non-associated flow rule or by applying strain-softening are very similar, which is not surprising since both models cause loss of ellipticity above some threshold stress level, but strain-softening is somewhat more tractable from a numerical point of view, since the governing tangential stiffness matrix remains symmetric.

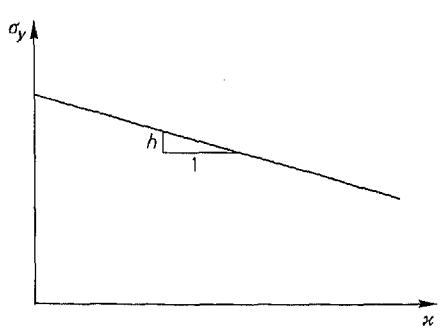

Fig. 2. Hardening diagram for strain-softening plasticity

The von Mises yield function is very convenient from a computational point of view, because the integration of the differential stress-strain relations over a finite loading step becomes appealingly simple and accurate for the Euler backward integration algorithm advocated in [10, 15, 16]. As demonstrated in [10], the Euler backward integration rule then reduces to the so-called elastic predictor-radial return method. We obtain for the new stress $\boldsymbol{\sigma}^1$ after integrating over a finite loading step

$$\boldsymbol{\sigma}^1 = \boldsymbol{\sigma}^t - \frac{3\mu}{h + 3\mu}\left(1 - \frac{\sigma_y(\varkappa)}{\sqrt{3J_2^t}}\right)\mathbf{s}^t \tag{20}$$

in which $\mathbf{s}$ contains the deviatoric stresses and the superscript t refers to the trial stress state, and where h is the plastic hardening modulus (negative in a strain-softening model) and μ is the elastic shear modulus. The elasto-plastic tangent operator that is consistent with this integration rule has first been given by Simo and Taylor [22] and reads

$$\mathbf{D} = \mathbf{D}^* - \frac{\mu^*}{1 + h^*/(3\mu^*)}\frac{\mathbf{s}\mathbf{s}^T}{J_2} \tag{21}$$

with $\mathbf{D}^*$ an elasticity matrix in which the shear modulus μ and Poisson's ratio ν are modified according to

$$\mu^* = \frac{E}{2(1+\nu) + 3E\,\Delta\varkappa/\sqrt{3J_2}}, \tag{22}$$

$$\nu^* = \frac{\nu + \frac{1}{2}E\,\Delta\varkappa/\sqrt{3J_2}}{1 + E\,\Delta\varkappa/\sqrt{3J_2}} \tag{23}$$

with Young's modulus E and the increase $\Delta\varkappa$ of the hardening parameter. The modified hardening modulus h^* is given by

$$h^* = \frac{h}{1 - E\,\Delta\varkappa/\sqrt{3J_2}}. \tag{24}$$

The so-called consistent tangent operator, as defined by (21)—(24), has been employed in all the analyses described in the sequel.

It is noted that the von Mises yield function has been used rather than the Tresca model. This is partly because the von Mises yield function is smooth (note however, that angular yield surfaces need not present such numerical difficulties as is sometimes suggested in the literature, provided that proper procedures are employed [10, 16]), and partly because use of the von Mises yield function allows comparison with some other analyses in the literature [7, 8, 23].

6 Bifurcation analysis of a biaxial test on strain-softening soil

In consideration of the questions posed in the analysis of the biaxial test on dry sand that has been described succinctly in the foregoing, a similar test will now be analyzed for the strain-softening von Mises plasticity model outlined in the preceding section. Two different discretizations have been used (Fig. 3) and 8-noded plane strain elements with a 9-point Gaussian integration rule have been employed. As in the analysis for the dry sand, the load has been applied by incrementing the force at the top of the sample, while dependence relations have been applied so as to ensure that all the nodes at the top undergo the same vertical displacement. All the points at the bottom as well as at the top of the specimen were free to move horizontally (perfectly smooth) except for the center node at the bottom which was fixed. Incrementation of the axial load was now started from a strain-free and stress-free state, since the cohesion of the material obviates the need for application of a confining stress. In all the analyses the shear modulus was taken as $\mu = 0.625\ \mathrm{N/mm^2}$. The initial yield stress was assumed to be $\sigma_y = 0.07\ \mathrm{N/mm^2}$, while linear softening was adopted thereafter.

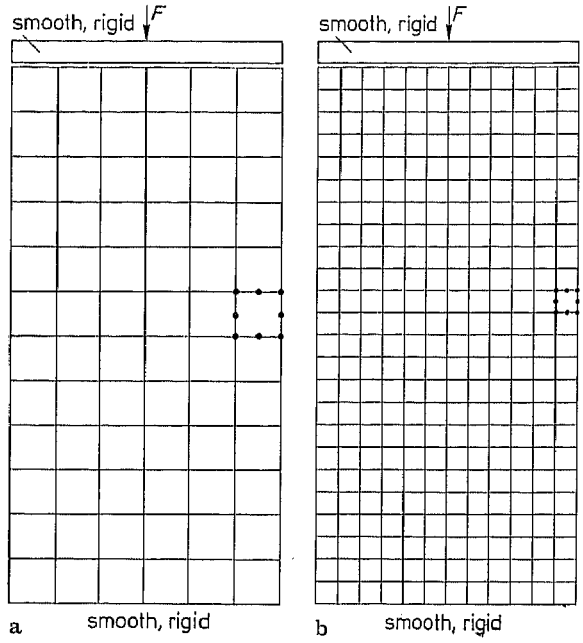

Fig. 3a and b. Quadrilateral elements; a coarse mesh of 72 8-noded elements, b fine mesh of 288 8-noded elements

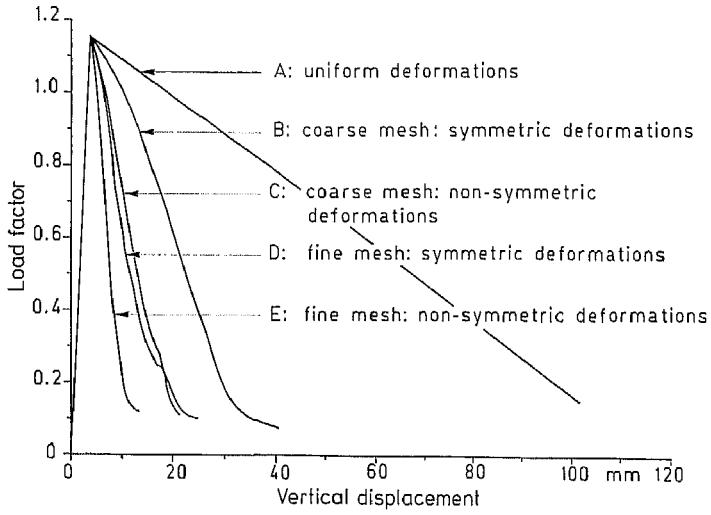

Fig. 4. Load versus vertical displacement of top nodes

After passing the peak of the load-deflection curve (Fig. 4) using indirect displacement control, an eigenvalue analysis has been carried out using a Jacobi-subspace method (e.g. [21]). The results have been plotted in Fig. 5 for $\nu = 0.49$ and $h/\mu = -0.1$. A total of 9 negative eigenvalues has been computed for this discretization and choice of material parameters. It is observed from Fig. 5, that eigenmodes that are symmetric with regard to the vertical centerline as well as eigenmodes that are unsymmetric with regard to this line are present. Furthermore, eigenmodes with a half wavelength as well as eigenmodes that show several wavelengths are observed. Effectively, the number of eigenmodes that is found is limited by the number of waves that can be accommodated within the finite element mesh. For the finer mesh of Fig. 3b 13 negative eigenvalues are found at this point, the additional eigenmodes showing a higher number of waves. A salient observation is, that a shear band mode is not found in either of the analyses.

Shear band modes were also not found when the material parameters were varied. Taking 0.4 for Poisson's ratio instead of 0.49 yielded more negative eigenvalues, namely 13, but a shear band mode could not be identified. The same is true when a steeper softening slope was used ($h/\mu = -0.2$). Again, 13 negative eigenvalues were extracted, but all the modes displayed a wave-pattern.

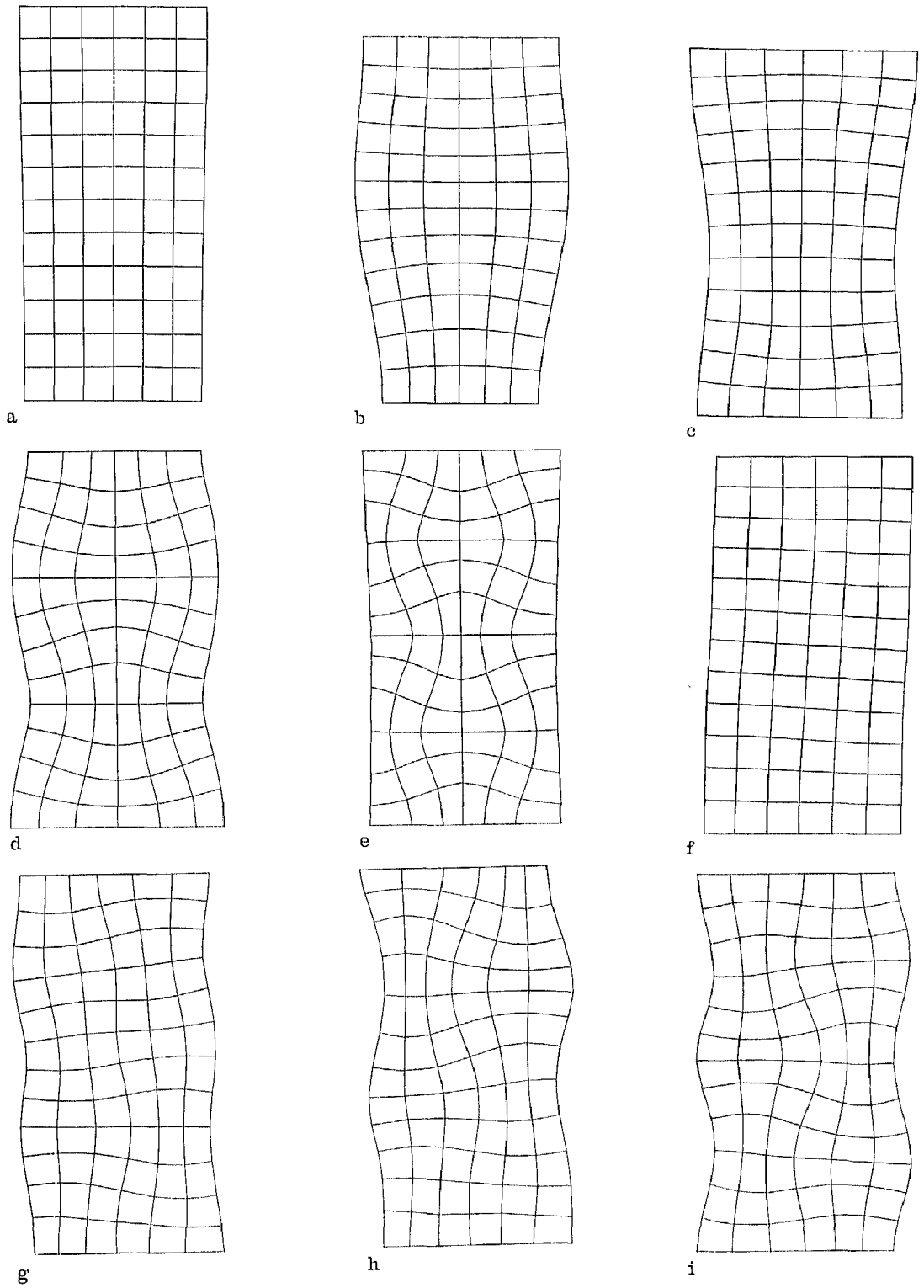

Fig. 5a–i. Eigenmodes for coarse mesh just beyond peak ($\nu = 0.49$ and $h/\mu = -0.1$)

Additional eigenstates are also generated when the boundary conditions put less restraint on the sample. For example, 10 negative eigenvalues are computed instead of 9 when the upper loading platen is allowed to rotate. Increasing the degree of kinematic restraint on the other hand decreases the number of negative eigenvalues. When analyzing the mesh of Fig. 3b with axisymmetric instead of plane strain elements, only 2 negative eigenvalues were calculated. One of the eigenvectors was a uniform extension mode, the other was a long-wave barrelling mode.

After the eigenvalue extraction, the incremental displacement vector was perturbed by one of the eigenvectors of Fig. 5. This resulted in a load-deflection path that runs much steeper than the reference curve for continuing homogeneous deformations, which was obtained on a single element (curve A in Fig. 4). Here, it made a major difference whether a symmetric or whether an asymmetric eigenmode was selected. When the eigenmode of Fig. 5i was used to perturb the solution with continuing homogeneous displacements, the curve that is labelled with C in Fig. 4 was obtained. Upon perturbation of the solution with the symmetric eigenmode of Fig. 5e the shallower curve B was obtained. A similar procedure for the uniformly refined mesh of Fig. 3b resulted in the curves D and E. Concentrating now on the results for the finer mesh, we observe that curve D is not the lowest branch and the tangent stiffness matrix on this path must therefore have at least two negative eigenvalues, one being related to the limit point, the other being related to the alternative (asymmetric) equilibrium state. On the other hand, the tangent stiffness matrix on path E should only have one negative eigenvalue. Both assertions were confirmed in eigenvalue analyses. It is interesting that one of the eigenmodes of the tangent stiffnex matrix is completely symmetric, while the other is asymmetric and thus related to the alternative equilibrium state.

7 Imperfection sensitivity

Inasmuch as symmetric eigenmodes can not trigger an asymmetric failure mode, so are symmetrically located imperfections unable to force a structure to fail asymmetrically. Consequently, a symmetric imperfection pattern will not cause that the steepest descending branch is computed after passing the limit point. Moreover, the purpose of inserting imperfections in a specimen, namely to transfer the limit problem into a bifurcation problem, may be missed altogether if no eigenvalue analyses are carried out. For instance, those analyses of Needleman and Tvergaard [5, 6], Prévost and Hughes [7, 8] and Leroy and Ortiz [24] in which symmetric imperfection patterns are applied, are basically still bifurcation analyses in which the lowest branch is not obtained. And if, as in some cases, an asymmetric failure mode is obtained in the calculation, this is simply caused by round-off error. Such a case should be treated with utmost care, since the results may then be unreproducable in the sense that on another computer, with for instance another machine precision, different results may be obtained.

The conclusions stated above can be drawn even further, since all plasticity models with a negative hardening modulus ($h < 0$), or even more generally all problems in which ellipticity is lost at some generic stage in the loading process, possess non-symmetric eigenmodes and failure will ultimately be asymmetric. So, making use of symmetry, but also of antisymmetry [14] or axisymmetry [26, 33], is pointless if we want to compute the post-peak behavior. Indeed, even for an ideally-plastic material ($h = 0$) the failure mode will eventually be non-symmetric, but the upper and lower bound theorems then guarantee that the limit load is unique, at least under the assumption of small displacement gradients [25]. A nice example is Prandtl's problem, where the Hill and the Prandtl mechanisms results in the same failure load.

To further analyze the role of imperfections, some additional analyses have been carried out for the finer mesh. In the first calculation two weak elements, that were located symmetrically with respect to the vertical centerline, were introduced in the finite element mesh. The initial yield stress of these elements was reduced by 1 percent. As the load was incremented, strain localization gradually progressed from the weak elements. After passing the limit point with increments of approximately 0.000 5 N/mm^2 an eigenvalue analysis was carried out for the tangent stiffness matrix. This resulted in two negative eigenvalues. The corresponding eigenmodes are shown in Fig. 6a and b. We observe a symmetric and an unsymmetric eigenmode. The symmetric

mode obviously corresponds to the limit behavior, while the unsymmetric mode relates to the bifurcation point that has been passed in the same small load increment. In order to substantiate this assertion further, an additional analysis has been undertaken for the same data and geometry, but with direct displacement control, i.e. in which all the vertical displacements of the top of the specimen were directly prescribed rather than applying a force and controlling the displacements by means of constraint equations. This analysis yielded a single negative eigenvalue for the stiffness matrix just beyond the maximum load level. Figure 6c shows that this eigenmode is unsymmetric and relates to the bifurcation point that has been passed. Note, however, that the displacements in both analyses remain completely symmetric with respect to the vertical centerline. This is shown in Fig. 7a, which shows the incremental displacements slightly beyond the maximum load. A third calculation with only one weak element yielded one negative eigenvalue for the stiffness matrix just beyond the peak load and resulted in the failure mode of Fig. 7b.

The terminology symmetrically located deserves some further explanation. It is implied that for an arbitrary structure, there must not exist a line with respect to which there is symmetry. For the example of a biaxial test two such lines exist, namely the vertical and the horizontal centerlines. Since the number of elements is even in the vertical direction, inserting weak elements automatically removes the symmetry with regard to the horizontal centerline. When we insert

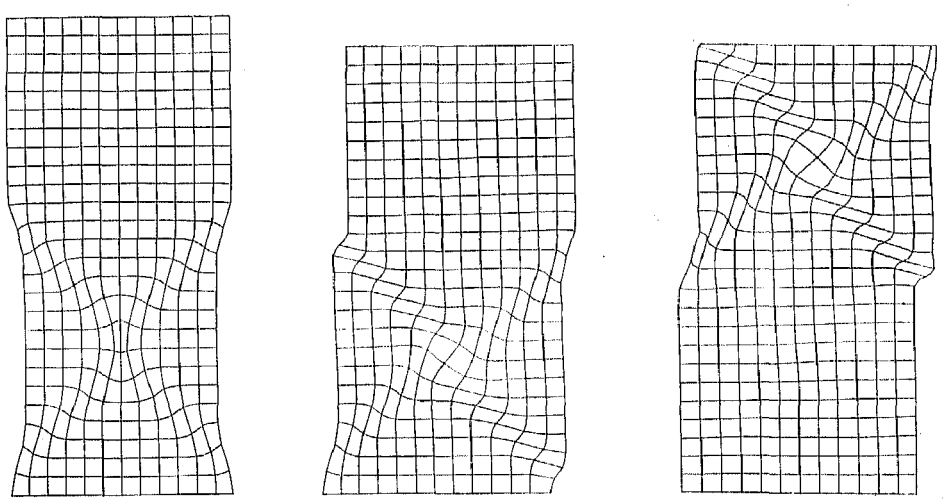

Fig. 6a–c. Eigenmodes for fine mesh after perturbation ($\nu = 0.49$ and $h/\mu = -0.1$); **a** first eigenmode, **b** second eigenmode, **c** eigenmode for direct displacement control

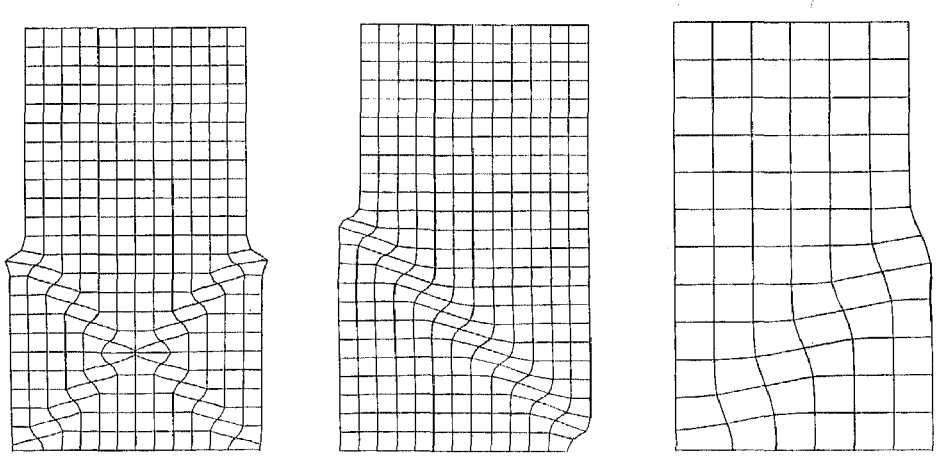

Fig. 7a–c. Incremental displacement field just beyond the limit point of curves in Fig. 4; **a** for fine mesh, and curve D, **b** for fine mesh and curve E, **c** for coarse mesh and curve C

two imperfection that are symmetrically located with respect to the vertical center line, we obtain a symmetric failure pattern that consists of two crossed shear bands, but when we insert an asymmetric imperfection, we get an asymmetric failure mode with a single shear band. Note that if the weak spots had been distributed such that vertical symmetry had not been disturbed either, a failure pattern of at least four crossed shear bands would have been computed. The number of negative eigenvalues on this branch would have been three and the load-deflection curve would, taking the coarse mesh as an example, have been approximately twice as shallow as curve *B* of Fig. 4.

The eigenmodes of Fig. 6 are also interesting in another respect. They show that finite elements can simulate highly localized deformation bands. Consequently, the fact that bifurcation modes which exhibit localized deformation bands were not found just beyond the peak load is not caused by an inability of finite elements to resolve such eigenmodes. We must rather conclude that they are simply not present in the model at that point. The reason for the discrepancy between the absence of localizations in the present numerical simulation and the prediction of them by the theoretical analysis of Rudnicki and Rice [1, 2], Vardoulakis et al. [3, 4], Vermeer [18] and Mandel [19], lies in the assumption of these authors that the discontinuity develops in an infinite medium. In a finite specimen shear bands need some time to develop because of the boundary conditions. This is evidenced by the observation that the plastic strains first accumulate in one corner which acts as a nucleus for the development of the deformation band. Depending on the precise formulation of the model the deformation band develops more or less gradually after passing the bifurcation point at which the diffuse modes become available.

It is finally noted that the very fact that eigenvalue analyses of the tangent stiffness matrix are necessary to verify that the lowest load-deflection branch has been calculated, casts some doubts on the usefulness of elastic stiffness approaches. The elastic stiffness method can not recognize eigenstates and simply picks a solution, but the analyst has no possibility to check whether it is the lowest branch.

8 Mesh sensitivity

Mesh refinement has a pathological influence on the results when strain-softening is incorporated in the employed constitutive model. This becomes apparent in three different ways, namely via the number of waves that can be resolved by the finite element mesh, through the load-deflection curve and in the failure mode.

The incremental displacement field at failure is probably the most striking example of the influence of the mesh refinement. Comparing the failure mode of the fine mesh with that of the coarser mesh (Fig. 7 b, c), we observe that in both cases the width of the shear zone is completely determined by the design of the finite element mesh and is approximately one element wide. Similar results have been found when studying shear band formation in metals [5, 6] and crack propagation in concrete [12—14, 26, 27].

The influence of mesh refinement on the load-deflection curve is depicted in Fig. 4, where a uniformly refined mesh yields a load-deflection curve that is roughly twice as steep as the original mesh. Interestingly, a load-deflection curve that is approximately twice as steep is also obtained when an asymmetric failure mode, with a single shear layer, is enforced instead of two crossed shear layers. Indeed, the curves *C* and *D* of Fig. 4 virtually coincide. Observations like this form the basis of energy approaches [26—28] that set out to achieve mesh-objectivity by controlling the amount of energy that is released in strain-softening solids. Such solutions, however, do not remedy the above mentioned excessive dependence of the failure mode on the mesh. Actually, this is not surprising, since the governing differential equations of the continuum are not changed by these models. Recently, there have been some attempts to enhance the continuum description, either via nonlocal approaches [29, 30], consideration of couple stresses [31] or inclusion of strain rate effects [32], so that the shear band thickness is embedded in the continuum description. Although some solutions have been published for these models, it does not seem possible as yet to indicate which approach will be most successful.

9 Strip-footing on strain-softening soil

The biaxial test that has been discussed in the preceding sections lends itself for a critical evaluation of the numerical procedures because much is known about the problem and because it is also analytically tractable. This is not true for another classical soil mechanics problem, namely the problem of a strip-footing on an infinite half-space. Finite element solutions of this problem have been generated before for elastic-plastic models with and without hardening and with associated and non-associated flow rules, e.g. [8, 15]. Solutions for strain-softening materials, however, are rare [34, 35], and invariably consider a symmetric part of the half-space. As suggested by the example of the biaxial test, restriction to a symmetric part of the half-space neglects the latent asymmetric solution and does not compute the lowest equilibrium branch.

In this section finite element solutions for the strip-footing problem are described in which no use has been made of possible symmetries in the finite element mesh (Fig. 8). The same material parameters that have been used in the analysis of the biaxial test have also been adopted in this analysis except for the fact that a shallower softening curve has been used: $h/\mu = -0.01$. The load has been applied to the center node of the footing (which is located on the line of symmetry) and dependence relations have been applied so as to ensure that the footing plate remains rigid. Note that this type of loading augmented with the constraint conditions will initially cause a uniform vertical displacement of the footing. Yet, the constraint conditions are such that rotation of the footing is not prevented. Furthermore, horizontal displacements of the nodes of the footing are allowed which implies that the footing is perfectly smooth.

The analysis resulted in a stable solution up to the limit point of the load-settlement diagram of Fig. 9. Immediately beyond the limit point, two negative pivots were found upon factorizing the tangent stiffness matrix. A subsequent eigenvalue analysis yielded a symmetric (Fig. 10a), and an asymmetric eigenmode (Fig. 10b), which clearly involves a rotation of the footing plate. Next, the incremental solution was perturbed by a part of the asymmetric eigenmode. A properly

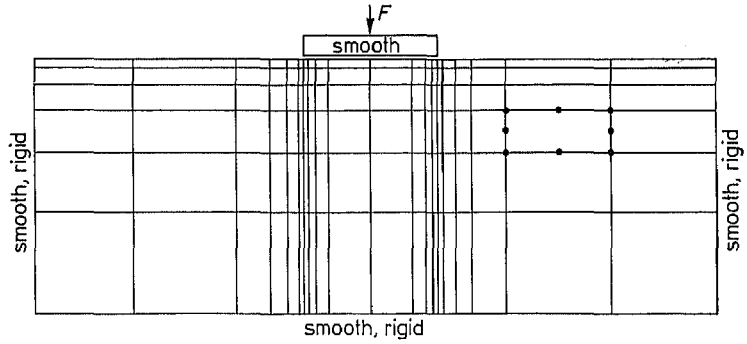

Fig. 8. Finite element mesh for strip-footing problem

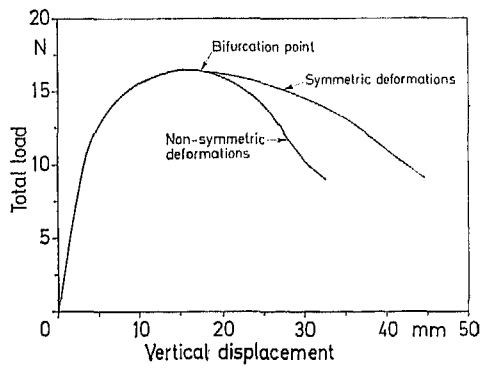

Fig. 9. Load-settlement curve for symmetric and asymmetric deformations

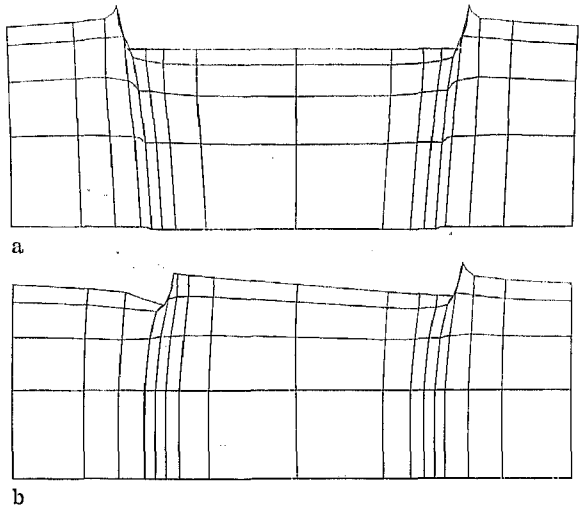

Fig. 10a and b. Eigenmodes at limit/bifurcation point for strip-footing problem (only a part of the mesh is shown); **a** symmetric eigenmode, **b** asymmetric eigenmode

converged solution was again obtained and resulted in the steeper post-peak curve of Fig. 9. The failure mode appeared to resemble the asymmetric eigenmode closely although the localization was even more pronounced.

In addition to the analysis for the full mesh an analysis for a symmetric half of the mesh has been undertaken. This resulted in the shallower post-peak curve. If the solution had not been perturbed by the asymmetric eigenmode at the peak load, this response would also have been obtained for the full mesh and two negative eigenvalues would have been extracted for the tangent stiffness matrix in the post-peak regime. The analysis for the strip footing therefore underscores the observations of the preceding sections, namely that making use of symmetries, or inserting symmetrically located imperfection patterns, does not transfer the bifurcation point into a limit point.

10 Concluding remarks

When carrying out a finite element analysis of a structure that is composed of a material that may, at a generic stage in the loading process, cause loss of ellipticity of the equations that describe the structural behavior, it is necessary to continuously check the lowest eigenvalues of the tangent stiffness matrix. When the lowest eigenvalue becomes negative on a monotonically rising branch of the load-deflection curve, or when multiple negative eigenvalues are extracted on a descending branch, a bifurcation point has been passed and the currently computed equilibrium state no longer corresponds to the lowest equilibrium branch. To return to this branch the current displacement increment must be perturbed by a portion of the eigenvector that corresponds to the lowest eigenvalue. The selection of how much the displacement increment must be perturbed is problem dependent and may be rather critical for some classes of problems. When a bifurcation occurs on a descending branch or near peak load, it may be difficult to reach the lower equilibrium state. This is particularly true for solids that display different behavior in loading and unloading, since the numerical procedure will then easily return to the unloading branch rather than result in an equilibrium state on the lower loading branch.

Inasmuch as keeping track of the stability of the equilibrium state requires computation of the current tangent stiffness matrix, we must continuously calculate this matrix already for this reason alone. Iterative procedures that circumvent calculation of the tangent stiffness, such as elastic stiffness methods, therefore seem misused in analyses which set out to compute the post-peak behavior of a soil mass.

The developed procedures are applied in a finite element analysis of a biaxial test on a strain-softening elasto-plastic solid. A whole set of eigenvalues and corresponding eigenvectors is calculated. The spectrum of eigenvectors features symmetric as well as unsymmetric eigenvectors. Only perturbation with an unsymmetric eigenvector will eventually lead to a non-symmetric failure mode with a single shear layer. Since this failure mode corresponds to the lowest post-peak equilibrium branch, it is evident that when symmetrically distributed imperfection patterns are used to trigger localization, only symmetric, crossed shear band patterns will be obtained. These failure modes do not correspond to the lowest equilibrium branch. To trace the lowest equilibrium branch, no symmetry, antisymmetry, or axisymmetry should be present in a model. Consequently, we can never make use of symmetry, antisymmetry, or axisymmetry when loss of ellipticity is to be expected at some stage of the loading process. This illustrates that it is necessary to have a possibility in a numerical code that can carry out a bifurcation analysis, since it is not always easy to a priori model a structure such that symmetry and antisymmetry are completely avoided.

The calculated eigenvectors show a number of diffuse bifurcation modes. Nonethelesse, a localized shear band mode is not obtained. This is because we have analyzed a finite specimen. The shear band analyses which predict shear band type instabilities at this point have been derived under the assumption of an infinitely thin shear band in an infinite medium, thus by-passing the effect that the boundary conditions have on postponing localization. In the numerical simulation it appears that prior to localization, plastic strains accumulate at some point of structure which acts as a starting point from which the shear bands propagate.

Acknowledgements

The examples reported in this paper have been calculated with the DIANA finite element code of the TNO Institute for Building Materials and Structures.

References

1. Rice, J. R.: The localization of plastic deformation. In: Koiter, W. T. (ed.) Proc. IUTAM Congress Delft, pp. 207–220. Amsterdam: North-Holland 1976
2. Rudnicki, J. W.; Rice, J. R.: Conditions of the localization of the deformation in pressure-sensitive materials. J. Mech. Phys. Solids 23 (1975) 371–394
3. Vardoulakis, I.; Goldscheider, M.; Gudehus, G.: Formation of shear bands in sand bodies as a bifurcation problem. Int. J. Numer. Anal. Methods Geomech. 2 (1978) 99–128
4. Vardoulakis, I.: Shear band inclination and shear modulus of sand in biaxial tests. Int. J. Numer. Anal. Methods Geochem. 4 (1980) 103–119
5. Needleman, A.; Tvergaard, V.: Finite element analysis of localization in plasticity. In: Oden, J. T.; Carey, G. F. (eds.) Finite elements: Special problems in solid mechanics, pp. 94–157. New Jersey: Prentice-Hall 1984
6. Tvergaard, V.; Needleman, A.; Lo, K. K.: Flow localization in the plane strain tensile test. J. Mech. Phys. Solids 29 (1981) 115–142
7. Prévost, J. H.; Hughes, T. J. R.: Finite element solution of elastic-plastic boundary value problems. J. Appl. Mech. 48 (1981) 69–74
8. Prévost, J. H.: Localization of deformation in elastic-plastic solids. Int. J. Numer. Anal. Methods. Geomech. 8 (1984) 187–196
9. Vermeer, P. A.; de Borst, R.: Non-associated plasticity for soils, concrete and rock. Heron 29 (1984) 1–62
10. de Borst, R.: Non-linear analysis of frictional materials. Dissertation, Delft University of Technology 1986
11. de Borst, R.: Bifurcations in finite element models with a non-associated flow law. Int. J. Numer. Anal. Methods. Geomech. 12 (1988) 99–116
12. de Borst, R.: Computation of post-bifurcation and post-failure behavior of strain-softening solids. Comput. Struct. 25 (1987) 211–224
13. Rots, J. G.; Hordijk, D. A.; de Borst, R.: Numerical simulation of concrete fracture in 'direct' tension. In: Luxmoore, A. R.; Owen, D. R. J.; Rajapakse, Y. P. S.; Kanninen, M. F. (eds.) Numerical methods in fracture mechanics, pp. 457–471. Swansea: Pineridge Press 1987
14. Rots, J. G.; de Borst, R.: Analysis of mixed-mode fracture in concrete. ASCE J. Eng. Mech. 113 (1987) 1739–1758

15. de Borst, R.; Vermeer, P. A.: Possibilities and limitations of finite elements for limit analysis. Géotechnique 34 (1984) 199—210
16. de Borst, R.: Integration of plasticity equations for singular yield functions. Comput., Struct. 26 (1987) 823—829
17. Ramm, E.: The Riks/Wempner approach — an extension of the displacement control method in nonlinear analyses. In: Hinton, E.; Owen, D. R. J.; Taylor, C. (eds.) Recent advances in non-linear computational mechanics, pp. 63—86. Swansea: Pineridge Press 1982
18. Vermeer, P. A.: A simple shear-band analysis using compliances. In: Vermeer, P. A.; Luger, H. J. (eds.) Proc. IUTAM Symp. deformation and failure of granular materials, pp. 493—499. Rotterdam: Balkema 1982
19. Mandel, J.: Conditions de stabilité et postulat de Drucker. In: Kravtchenko, J.; Sirieys, P. M. (eds.) Proc. IUTAM Symp. on rheology and soil mechanics, pp. 58—68. Berlin: Springer 1966
20. Needleman, A.: Non-normality and bifurcation in plane strain tension and compression. J. Mech. Phys. Solids 27 (1979) 231—254
21. Bathe, K. J.: Finite element procedures in engineering analysis. New Jersey: Prentice-Hall 1982
22. Simo, J. C.; Taylor, R. L.: Consistent tangent operators for rate-independent elasto-plasticity. Comput. Methods Appl. Mech. Eng. 48 (1985) 101—118
23. Bardet, J. P.: A note on the finite element simulation of strain localization. In: Pande, G. N.; Middleton, J. N. (eds.) NUMETA 1987, vol. 2. Transient/dynamic analysis and constitutive laws for engineering materials, Paper C21. Dordrecht: Martinus Nijhoff 1987
24. Leroy, Y.; Ortiz, M.: Finite element analysis of strain localization in frictional materials. Int. J. Num. Anal. Meth. Geomech. 12 (1988)
25. Koiter, W. T.: General theorems for elastic-plastic solids. In: Sneddon, I. N.; Hill, R. (eds.) Progress in solid mechanics, vol. 1, pp. 167—221. Amsterdam: North-Holland 1960
26. Willam, K. J.; Hurlbut, B.; Sture, S.: Experimental, constitutive and computational aspects of concrete failure. In: Preprints US-Japan Seminar on finite element analysis of reinforced concrete structures pp. 149—172. New York: ASCE 1985
27. Bazant, Z. P.; Oh, B.: Crack band theory for fracture of concrete. RILEM Materials and Structures 16 (1983) 155—177
28. Pietruszczak, S.; Mróz, Z.: Finite element analysis of deformation of strain-softening materials. Int. J. Numer. Methods. Eng. 17 (1981) 327—334
29. Bazant, Z. P.; Belytschko, T. B.; Chang, T.-P.: Continuum theory for strain softening. ASCE J. Eng. Mech. 110 (1984) 1666—1692
30. Schreyer, H. L.; Chen, Z.: One-dimensional softening with localization. J. Appl. Mech. 53 (1986) 791 to 979
31. Mühlhaus, H. B.: Shear band analysis in granular material by Cosserat theory. In: Pande, G. N.; van Impe, W. F. (eds.) Numerical models in geomechanics, pp. 115—122. Redrudth: Jackson & Sons 1986
32. Needleman, A.: Material rate dependence and mesh sensitivity in localization problems. Comput. Methods Appl. Mech. Eng. 67 (1988) 69—86
33. Ottosen, N. S.: Evaluation of concrete cylinder tests using finite elements. ASCE J. Eng. Mech. 110 (1984) 465—481
34. Pietruszczak, S.; Stolle, D. F. E.: Deformation of strain softening materials. Part I: Objectivity of finite element solutions based on conventional strain softening formulations. Comput. Geotechnics (1985) 99—115
35. Runesson, K.; Samuelsson, A.; Bernsprang, L.: Numerical technique in plasticity including solution advancement control. Int. J. Numer. Methods Eng. 22 (1986) 769—788

Received May 24, 1988

Prof. Dr. ir. R. de Borst
TNO Institute for Building Materials and Structures
Delft University of Technology
P.O. Box 49
NL-2600 AA Delft
The Netherlands